arXiv:1210.7201v1 [cond-mat.str-el] 26 Oct 2012

Finite temperature crossovers and the quantum Widom line near the Mott transition

J. Vučičević,[1] H. Terletska,[2] D. Tanasković,[1] and V. Dobrosavljević[3]

[1]*Scientific Computing Laboratory, Institute of Physics Belgrade,*
University of Belgrade, Pregrevica 118, 11080 Belgrade, Serbia
[2]*Condensed Matter Physics and Materials Science Department,*
Brookhaven National Laboratory, Upton, New York 11973, USA
[3]*Department of Physics and National High Magnetic Field Laboratory,*
Florida State University, Tallahassee, Florida 32306

We explore the recently established quantum critical region above the critical end-point in the half-filled Hubbard model. The resistivity displays characteristic quantum critical scaling near the instability line which we interpret as the quantum Widom line, in a close analogy with the Widom line in classical phase transitions. This line is determined by the minimum curvature of the free energy functional and represents a continuation of the line of the first order phase transition. The quantum Widom line, however, does not require the existence of the first order phase transition. It is rather a consequence of the zero temperature quantum phase transition, which in our case is masked by the phase coexistence region. Along the quantum Widom line the density of states is reduced, but the insulating gap is not yet fully open. We contrast this line with the Fermi liquid coherence line which is the boundary of the existence of long-lived quasiparticles.

I. INTRODUCTION

Strongly correlated materials exhibit a variety of phases whose properties often lack a complete microscopic understanding.[1] While transport and thermodynamic properties near the quantum critical point depend on details of the system under consideration, at higher temperatures they share many common features. A number of scaling hypotheses, based on the experimental data or theoretical models, are proposed to describe the "high-temperature" region of the phase diagram dominated by the incoherent excitations.[2–7]

Recently we have established a remarkable scaling of the resistivity curves above the critical end-point in the frustrated Hubbard model around the *instability line*, which is determined by the minimum curvature of the free energy functional.[8] The resistivity around this line exhibits a characteristic "fan-shaped" form, surprisingly similar to some experimental findings,[2] reflecting a gradual crossover from metallic to insulating transport. The scaling behavior in this high-temperature crossover regime is interpreted as an evidence of a hidden Mott quantum criticality, and it is argued that it incorporates universal features of transport in various materials.

In this paper we explore different regimes in the dynamical mean field theory (DMFT) phase diagram of the single band Hubbard model in the paramagnetic phase and carefully characterize relevant crossover lines. The instability line[8] separating the metallic and insulating transport is interpreted as a *quantum Widom line* (QWL). It is analogous to the Widom line at the crossover between liquid-like and gas-like behavior in supercritical fluids.[9] The quantum Widom line represents a continuation of the line of the first order phase transition and roughly follows the insulating spinodal on the metal-insulator transition (MIT) phase diagram. Along the quantum Widom line the density of states is reduced, but the insulating gap is not yet fully open. We contrast this line with the Fermi liquid coherence line which is the boundary of the existence of long-lived quasiparticles and follows a direction of the metallic spinodal.

The remaining part of the paper is organized as follows. Section II contains the phase diagram featuring various transport regimes and crossover lines. In Section III an explicit procedure for a determination of the quantum Widom line is given and its physical meaning is further illustrated. Section IV shows contour plots of the resistivity and β-function in the whole phase diagram and Section V contains the conclusions.

II. PHASE DIAGRAM AND CROSSOVER LINES

We consider a single band Hubbard model at half-filling

$$H = -\sum_{<i,j>\sigma} t_{ij}\left(c^{\dagger}_{i\sigma}c_{j\sigma} + c.c.\right) + \sum_{i} U n_{i\uparrow}n_{i\downarrow}, \quad (1)$$

where $c^{\dagger}_{i\sigma}$ and $c_{i\sigma}$ are the electron creation and annihilation operators, $n_{i\sigma} = c^{\dagger}_{i\sigma}c_{i\sigma}$, t_{ij} is the hopping amplitude, and U is the repulsion between two electrons on the same site. We use a semicircular density of states, and the corresponding half-bandwidth $D = 2t$ is set to be our energy unit. We focus on the paramagnetic DMFT solution, which is formally exact in the limit of large coordination. The DMFT is a unique method which studies the Fermi liquid low temperature region, the high-temperature incoherent transport and the Mott MIT within a single theoretical framework, and it is most reliable precisely at high temperatures when the correlations are more local.[7,10] To solve the DMFT equations we use the iterated perturbation theory[11] (IPT) and cross-check our results with numerically exact continuous time quantum Monte Carlo (CTQMC)[12,13], as shown in the Appendix.

The phase diagram in the $U-T$ plane, Fig. 1, shows several regimes and crossover lines. The Fermi liquid (FL) region is restricted to small interaction U and low temperatures. The boundary of this region is determined by a temperature up to which the resistivity follows usual $\rho \propto T^2$ behavior (pink dotted line). This happens approximately until the resistivity reaches a value $0.1\rho_{_{Mott}}$, where $\rho_{_{Mott}}$ is the maximal metallic resistivity in the semiclassical Boltzmann theory, which corresponds to the scattering length of one lattice spacing.[14] This criterion defines the boundary of the FL region and the corresponding temperature T_{FL} (see also Section IV). Above the FL crossover line the excitations gradually become more incoherent until the systems enters deep into the bad metal region with $\rho > \rho_{_{Mott}}$. It is interesting that the Drude-like quasiparticles exist for temperatures substantially larger than T_{FL}, up to the resistivity $\rho \sim \rho_{_{Mott}}$,[4] similar to the doped Hubbard model.[15] In the half-filled model the metallic resistivity can reach values an order of magnitude larger than the $\rho_{_{Mott}}$ due to the opening of the pseudogap at the Fermi level.[4]

It was recognized early on[16,17] that there are two distinct crossover lines in the DMFT phase diagram. Apart from the Fermi liquid coherence line which follows the linear part the metallic spinodal, there is another crossover line - extension of the insulating spinodal, which marks a crossover from the bad metal to the activated transport regime.[16,17] By analogy[18,19] to the familiar liquid-gas transition, we determine the precise location of such an "instability trajectory" (green dotted line on Fig. 1) by examining the curvature of the corresponding free energy functional.[20] This curvature vanishes at T_c and is finite and minimal at $T > T_c$, along this instability line. Consequently, our problem is recast as an eigenvalue analysis of the corresponding free energy functional $\mathcal{F}[G(i\omega_n)]$ for which the DMFT Green's function solution $G_{DMFT}(i\omega_n)$ represents a local extremum.[18,20,21] The resistivity around such an instability line exhibits a remarkably scaling with a power law dependence of the scaling parameter,[8] as expected in presence of *quantum criticality*. The boundary of the quantum scaling region is marked by green dashed lines (see Section III and Appendix B).

In a close analogy with the Widom line which marks a crossover between a liquid-like and gas-like behavior in supercritical fluids,[9] we name the line which determines the boundary between a metallic and an insulating behavior a *quantum Widom line*. There is, however, an important distinction: the Widom line is a consequence of the first order classical phase transition and it represents a continuation of the first order phase transition line to higher temperatures. Its quantum analog, the QWL, does not require the existence of the first order phase transition. It is rather a consequence of the zero temperature quantum phase transition, which is in the case that we study, masked by the phase coexistence region.

We emphasize that the immediate vicinity $T \approx T_c$ of the critical end-point has been carefully studied theoretically[18,22], and even observed in experiments[5], revealing classical Ising scaling (since one has a finite temperature critical point) of transport in this regime. In our study, we examine the crossover behavior at much higher temperatures $T \gg T_c$, displaying very different behavior: precisely what is expected in presence of quantum criticality. The existence of several scaling regimes is well known in a study of quantum phase transitions.[23] The peculiarity of our scaling analysis stems from a definition of the QWL motivated from the physics of classical liquid-gas phase transition.

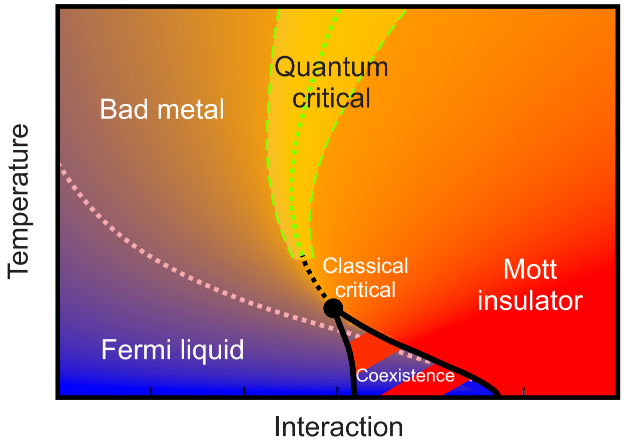

FIG. 1: Phase diagram of the half-filled Hubbard model. Color in the background is the actual result for the resistivity: blue color - small resistivity, red color - large resistivity.

III. QUANTUM WIDOM LINE

In this Section we present details of the procedure that we use to precisely determine the quantum Widom line. We further motivate the proposed term for this crossover line between a (bad) metal and an insulator by analyzing the resistivity and the density of states along the QWL. We explicitly show how several other popular definitions for the crossover line essentially reduce to the Fermi liquid coherence line, in a sharp contrast to the QWL.

A. Eigenvalue analysis of the free energy curvature

In order to reveal the proper scaling behavior close to the critical end-point, one has to follow a set of trajectories parallel to "zero field" trajectory $U_{WL}(T)$, and $\delta U \equiv U - U_{WL}(T)$ is expected to play the role of the scaling variable corresponding to a symmetry-breaking field favoring one of the two competing (metal vs. insulator) phases. By analogy[18,19] to the familiar liquid-gas transition, we determine the precise location of such an "instability trajectory" by finding the minimum of the curvature of the corresponding free energy functional[20]. The free energy near such an extremum can be written

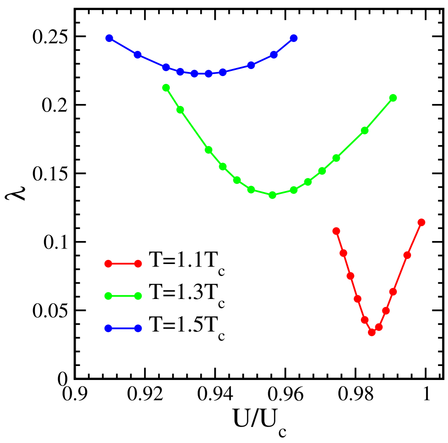

FIG. 2: Eigenvalue analysis: values for λ are plotted as a function of interaction at three different temperatures. The positions of the minima of these curves determine the instability line $U_{WL}(T)$ (quantum Widom line) along which the curvature of the free energy is minimal.

as

$$\mathcal{F}[G(i\omega_n)] = \mathcal{F}_0 + Tt^2 \sum_{m,n} \delta G(i\omega_m) M_{mn} \delta G(i\omega_n) + \dots , \tag{2}$$

where

$$M_{mn} = \frac{1}{2Tt^2} \left. \frac{\partial^2 \mathcal{F}[G]}{\partial G(i\omega_m) \partial G(i\omega_n)} \right|_{G=G_{DMFT}} \tag{3}$$

and $\delta G(i\omega_n) \equiv G(i\omega_n) - G_{DMFT}(i\omega_n)$. The curvature of the free energy functional is determined by the lowest eigenvalue λ of the fluctuation matrix M. As explained in Appendix A, λ can be obtained from the iterative solution of DMFT equations. The difference of the Green's functions in iterations n and $n+1$ of the DMFT self-consistency loop is given by

$$\delta G^{(n+1)}(i\omega_n) - \delta G^{(n)}(i\omega_n) = e^{-n\lambda} \delta G^{(0)}(i\omega_n) \tag{4}$$

and therefore λ determines the rate of convergence of the Green function to its solution.

An example of our calculations is shown on Fig. 2, where the eigenvalues at several temperatures are plotted as a function of interaction U/U_c. The minima of these curves define the locus of the instability trajectory $U_{WL}(T)$, which terminates at the critical end-point (U_c, T_c). The free energy curvature analysis can be used to pinpoint the position of the critical end-point from the high-temperature data. In this way, one does not need to study for this purpose the coexistence region below T_c, which in some cases may be accompanied by numerical difficulties.

The resistivity scaling procedure is presented in many details in Ref. 8. We first divide each resistivity curve by the resistivity along the QWL (the "separatrix") $\rho_{WL}(T) = \rho(T, \delta U = 0)$, and then rescale the temperature for each curve with an appropriately chosen parameter $T_0(\delta U)$ to collapse the data onto two branches. The family of resistivity curves displays characteristic quantum critical scaling of the form

$$\rho(T, \delta U) = \rho_{WL}(T) f(T/T_o(\delta U)), \tag{5}$$

with $T_o(\delta U) \sim |\delta U|^{z\nu}$, and $\rho_{WL}(T) \sim T$, with the exponent $z\nu \approx 0.56$. The scaling parameter T_o displays power law scaling with the same exponents for both scaling branches and falls sharply as $U \to U_{WL}$, which is consistent with quantum critical scenario and presents a stringent test of our scaling hypothesis. In Appendix C we show the scaled curves for a broad region on the phase diagram around the QWL, and identify the scaling region corresponding to the dashed lines in Fig. 1.

B. Density of states and resistivity along the QWL

The quantum Widom line physically represents a boundary between a metallic and insulating transport. This can be also seen from the density of states (DOS) along the QWL and its vicinity. Middle column on Fig. 3 shows the DOS along the QWL for three different temperatures. While the DOS at the Fermi level is strongly suppressed, the gap is not yet fully open. Left column shows the density of states in the metallic phase: there is a clear Drude peak at low temperatures, which gradually disappears as the bad metal region is reached by increasing the temperature. At larger U the system is in the insulating phase with fully open Mott gap, featuring activated transport.

It is also interesting to examine the resistivity along the QWL. Its values largely exceeds the Mott limit, yet it displays metallic-like but non-Fermi liquid-like temperature dependence $\rho_{WL}(T) \sim T$, Fig. 4. Such puzzling behavior, while inconsistent with any conventional transport mechanism, has been observed in several strongly correlated materials close to the Mott transition[14,24]. Our results thus suggest that it represents a generic feature of Mott quantum criticality.

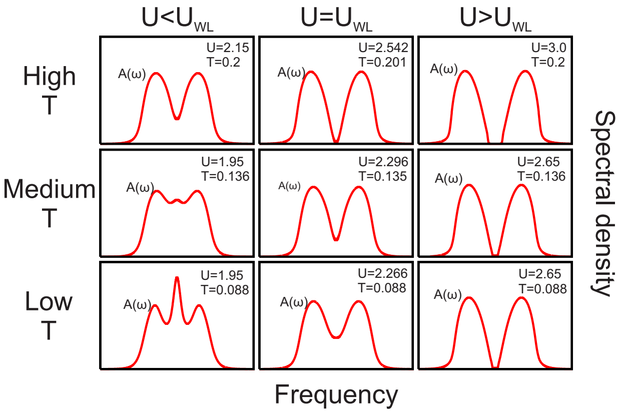

FIG. 3: Density of states around the Widom line. Along the Widom line (middle column) the DOS is strongly reduced at the Fermi level but the Mott gap is not yet fully open.

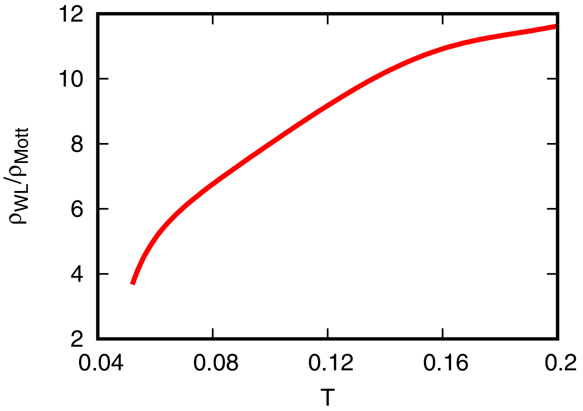

FIG. 4: Resistivity along the quantum Widom line.

C. Fermi liquid coherence line vs. QWL

In order to highlight the difference between the quantum Widom line and several other crossover lines often used in the literature,[25,26] we plot them together on Fig. 5. Light blue line (a) corresponds to $\rho = 0.1\rho_{Mott}$ and it is roughly the Fermi liquid coherence boundary up to which the resistivity follows $\rho \propto T^2$. At the orange line (b) the imaginary part of the self-energy at two lowest Matsubara frequencies becomes flat. Green line (c) is determined as the inflection point of the spectral density at the Fermi level with respect to the temperature, $d^2A(\omega = 0)/dT^2 = 0$, and dark blue line (d) corresponds to the inflection point of the resistivity, $d^2\rho(\omega = 0)/dT^2 = 0$). All of these four lines essentially correspond to a crossover between a Fermi liquid and bad metallic transport. In a sharp contrast, the quantum Widom line, red line (e), determines a boundary between the metallic and the insulating transport.

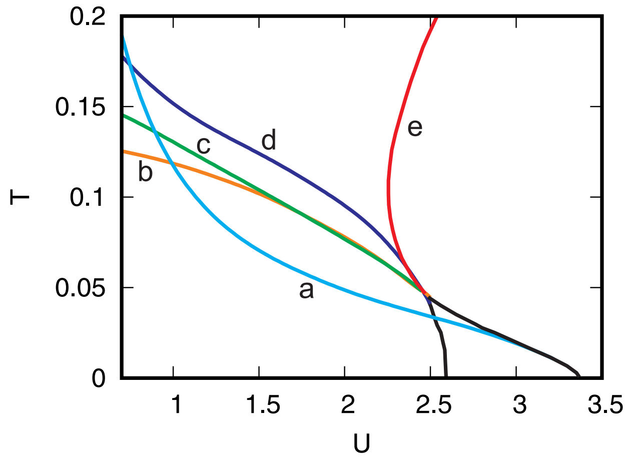

FIG. 5: Various definitions of the crossover lines. Lines (a)-(d) (see the text) essentially correspond to the FL coherence line are in sharp contrast to the QWL (e).

IV. RESISTIVITY AND β-FUNCTION

In this Section we plot the resistivity and the β-function in the entire $U - T$ plane. While these plots do not directly convey any new physical conclusions, they are valuable since they do not include any data analysis and are, therefore, completely unbiased to any physical concept. The DMFT expression for the resistivity, $\rho = 1/\sigma(\omega \to 0)$, is obtained from[11]

$$\sigma = \pi\sigma_0 \int_{-\infty}^{+\infty} d\varepsilon v^2(\varepsilon) D^0(\varepsilon) \int_{-\infty}^{+\infty} (-\frac{df}{d\omega} A^2(\varepsilon,\omega)), \quad (6)$$

where $A(\varepsilon, w) = -\frac{1}{\pi} ImG(\varepsilon, w)$, $v(\varepsilon) = \sqrt{(4t^2 - \varepsilon^2)/3}$. $D^0(\varepsilon) = \frac{1}{2\pi t^2}\sqrt{4t^2 - \varepsilon^2}$ is the noninteracting DOS, and f is the Fermi function.

The result is shown on the contour plot on Fig. 6 (resistivity is again given in units of ρ_{Mott}). The white stripes follow the lines of equal resistivity and approximately separate orders of magnitude in the resistivity. In the high-temperature region they emanate from the critical end-point (U_c, T_c), which is reminiscent to the quantum criticality.

To specify the scaling behavior, one usually computes the corresponding β-function[3] $\beta(g) = d\ln g/d\ln T$, with $g = \rho_{WL}/\rho$ being the inverse resistivity scaling function. As we have shown in Ref. 8, it displays a nearly linear dependence on $\ln g$, and is continuous through $\delta U = 0$ indicating precisely the same form of the scaling function on both sides of the transition - another feature exactly of the form expected for genuine quantum criticality. This functional form is very natural for the insulating transport, as it is obtained even for simple activated behavior $\rho(T) \sim e^{-E_g/T}$. The fact that the same functional form persists well into the metallic side is a surprise, especially since it covers almost an order of magnitude for the resistivity ratio. Such a behavior has been interpreted[3] to reflect the strong coupling nature of the critical point, which presumably is governed by the same physical processes that dominate the insulator. This points to the

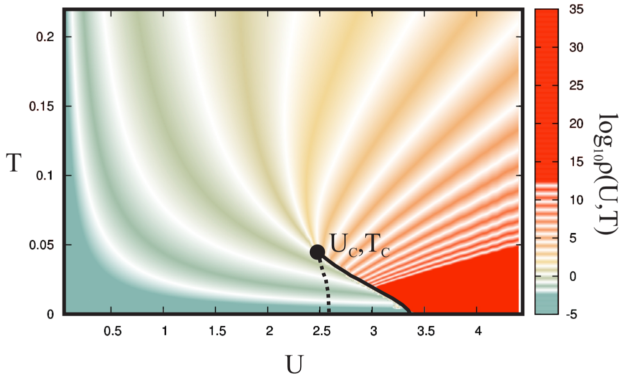

FIG. 6: Resistivity calculated in the entire $U - T$ plane. The white stripes follow the lines of equal resistivity and approximately separate orders of magnitude in the resistivity.

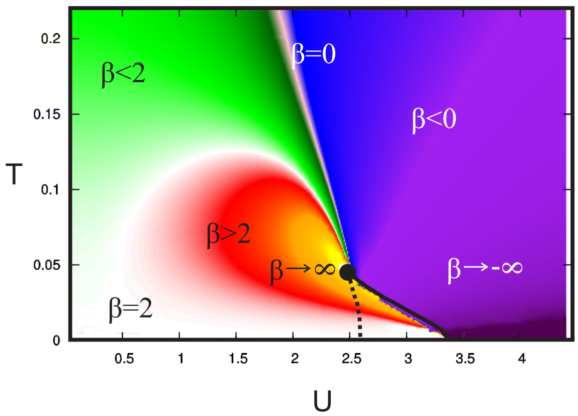

FIG. 7: The β-function calculated in the entire $U-T$ plane illustrates the different transport regimes.

fact that our QC behavior has a strong coupling, i.e. non-perturbative character.

The β-function,

$$\beta = \frac{d\log\rho}{d\log T}, \tag{7}$$

can be also used to illustrate different transport regimes on the phase diagram. The white region on Fig. 7 corresponds to the Fermi liquid regime where $\rho \sim T^2$. At higher temperatures (the green region) resistivity growth slows down; precisely in the critical point, β diverges (yellow) and in its near vicinity, a growth faster than quadratic is found (red). The pink line corresponds to the resistivity maxima where $\beta = 0$. At the insulating side of the transition, the resistivity is exclusively decreasing with increasing temperature and β is always negative (blue). Deep in the Mott insulator one finds the activating regime in which resistivity grows exponentially with decreasing temperature and at $T = 0$, β goes to $-\infty$ (purple).

V. CONCLUSIONS

In summary, we have explored in detail different regimes in the DMFT phase diagram of half-filled frustrated Hubbard model, with a careful analysis of relevant crossover lines. The line which separates metallic and insulating transport is characterized as a quantum Widom line in a close analogy with the liquid-gas crossover in supercritical fluids, and it is defined as the line of the smallest curvature of the free energy functional. This line starts from the critical end-point (U_c, T_c) on the phase diagram, where the curvature of the free energy functional goes to zero. The quantum Widom line, however, does not require the existence of first order phase transition. It rather emanates from the zero temperature metal-insulator transition, which is in the case of the Hubbard model masked by the phase coexistence region.

We have established a remarkable resistivity scaling around the QWL with a power law scaling parameter, as expected from the quantum criticality. We believe that the proposed concept is relevant for many systems near the Mott metal-insulator transition, and it can be tested on e.g. various organic Mott systems[6] where T_c is sufficiently bellow room temperature. A stringent test for our theory will be on the models where T_c can be significantly reduced[27] and where we expect that the quantum critical region extends to the lowest temperatures.

Acknowledgments

We thank A. Amaricci, M. Civelli, S. Florens, A. Georges, K. Haule, M. Jarrell, G. Kotliar, L. de' Medici, M. Rozenberg, T. Senthil, G. Sordi, J. M. Tremblay, and M. Vojta for useful discussions. J.V. and D.T. acknowledge support from the Serbian Ministry of Education and Science under project No. ON171017. V.D. was supported by the National High Magnetic Field Laboratory and the NSF Grant No. DMR-1005751, and H.T. by the DOE BES CMCSN grant DE-AC02-98CH10886. Numerical simulations were run on the AEGIS e-Infrastructure, supported in part by FP7 projects EGI-InSPIRE, PRACE-1IP and HP-SEE.

Appendix A: Eigenvalue analysis

The minimum curvature of the free energy functional for a given temperature is determined as follows. For simplicity we concentrate on the Bethe lattice. The Ginzburg-Landau free energy functional $F(\vec{G})$ in the Hilbert space of the Matsubara Green's functions $\vec{G} \equiv G(i\omega_n)$ is given by[11,18,20]

$$\begin{aligned} F(\vec{G}) &= -Tt^2\vec{G}^2 + F_{imp}(\vec{G}) \\ &= -Tt^2\sum_n G^2(i\omega_n) + F_{imp}(\vec{G}), \end{aligned} \tag{A1}$$

where the first term is the energy cost of forming the Weiss field $\vec{\Delta} = t^2\vec{G}$ around a given site, while the second term is the free energy of an electron at this site in the presence of the Weiss field.

Close to a local extremum $\vec{G}_0$, we can Taylor expand $F(\vec{G})$ in terms of deviation, $\delta\vec{G} = \vec{G} - \vec{G}_0$, from this point

$$\begin{aligned} F(\vec{G}) &= F(\vec{G}_0) + Tt^2\sum_{mn}\delta G(i\omega_m)M_{mn}\delta G(i\omega_n) + \ldots \\ &= F(\vec{G}_0) + Tt^2\,\delta\vec{G}\hat{M}\delta\vec{G} + \ldots \end{aligned} \tag{A2}$$

where

$$M_{mn} = \frac{1}{2Tt^2}\left.\frac{\partial^2 F(\vec{G})}{\partial G(i\omega_n)\partial G(i\omega_m)}\right|_{\vec{G}=\vec{G}_0}. \tag{A3}$$

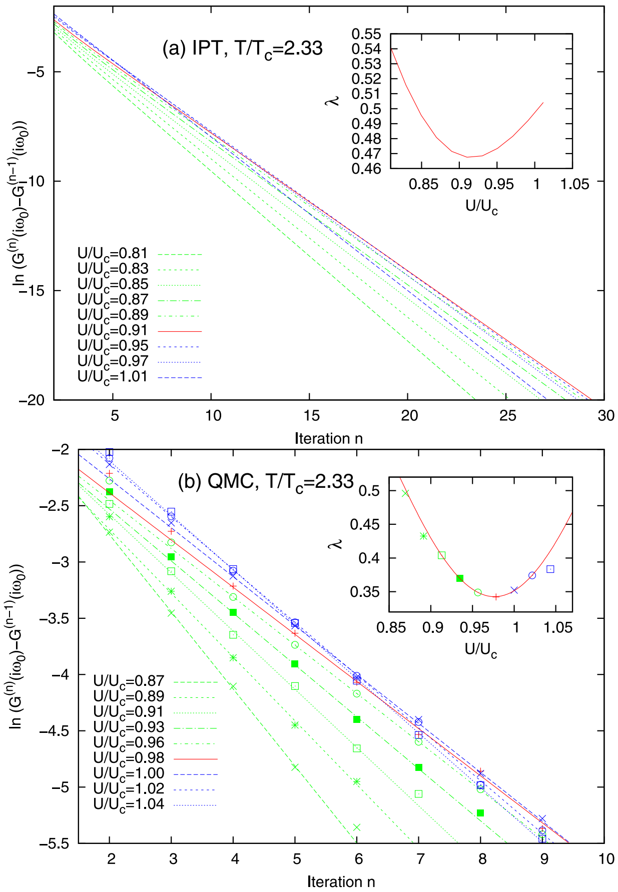

FIG. 8: Convergence rate in the iterative solution of DMFT equations at $T/T_c = 2.33$ using IPT impurity solver, panel (a), and CTQMC impurity solver, panel (b). The dashed lines in panel (b) are linear fits to the data. The insets are the corresponding eigenvalues determined by the slopes from the main panels.

We introduce a gradient function

$$\vec{g}(\vec{G}) \equiv \frac{1}{2Tt^2}\frac{\partial F(\vec{G})}{\partial \vec{G}} = \hat{M}\delta\vec{G} \tag{A4}$$

and define an iteration-substitution procedure by

$$\delta\vec{G}^{(n+1)} = \delta\vec{G}^{(n)} - \vec{g}(\vec{G}^{(n)}), \tag{A5}$$

which gives the minimum of the free energy as the iteration step $n \to \infty$. In the case of the free energy functional given by Eq. (A1), we have

$$\vec{g}(\vec{G}) = \vec{G}_{imp}(\vec{G}) - \vec{G}, \tag{A6}$$

and in the iterative procedure the Green's function converges to the minimum of the free energy which is at the same time also a self-consistent solution of the DMFT equations, given by the relation $G_{imp}(i\omega_n) = G(i\omega_n)$.

The curvature of the free energy for interaction U and temperature T can be obtained as follows. The eigenbasis $\vec{G}_\alpha$ and eigenvalues λ_α of matrix $\hat{M}$ are defined by

$$\hat{M}\vec{G}_\alpha = \lambda_\alpha\vec{G}_\alpha. \tag{A7}$$

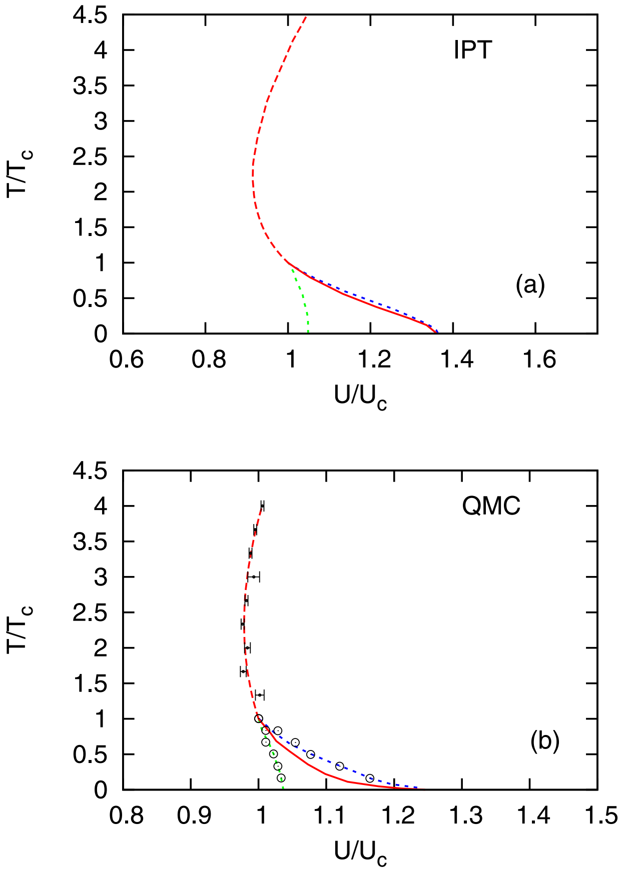

FIG. 9: Phase diagram obtained with IPT, panel (a), and CTQMC, panel (b). Temperature and interaction are scaled by their values at the critical endpoint ($T_c^{IPT} = 0.046$, $T_c^{QMC} = 0.03$ and $U_c^{IPT} = 2.472$, $U_c^{QMC} = 2.3$). Red dashed line is the instability line $U^*(T)$, full red line is the line of the first order MIT, and green and blue dotted lines are left and right spinodals.

We can expand $\delta\vec{G}^{(n)}$ as

$$\delta\vec{G}^{(n)} = \sum_\alpha a_\alpha^{(n)}\vec{G}_\alpha \tag{A8}$$

where $a_\alpha^{(n)}$ are the coefficients of $\delta\vec{G}^{(n)}$ in the eigenvalue basis. Substituting into Eq. (A5), one obtains

$$\delta\vec{G}^{(n)} = \sum_\alpha e^{-nB_\alpha} a_\alpha^{(0)}\vec{G}_\alpha, \tag{A9}$$

where

$$B_\alpha = -\ln(1-\lambda_\alpha). \tag{A10}$$

For large n the term with lowest $B_\alpha = B_{\alpha_0}$, which corresponds to the lowest eigenvalue $\lambda_{\alpha_0} \equiv \lambda$, is dominant

$$\delta\vec{G}^{(n)} = e^{-nB_{\alpha_0}} a_{\alpha_0}^{(0)}\vec{G}_{\alpha_0}, \quad n \gg 1. \tag{A11}$$

Here α_0 is the coefficient corresponding to the Green function with the lowest eigenvalue λ. Now it is obvious that through iterations, the solution $\vec{G}$ approaches to $\vec{G}_0$ exponentially along a direction defined by the eigenvector of $\hat{M}$ corresponding to its minimal eigenvalue λ. The coefficient B_{α_0} and the corresponding eigenvalue λ are then obtained from the slope in the iterative relation

$$\ln\left[G(i\omega_n)^{(n+1)} - G(i\omega_n)^{(n)}\right] = const - nB_{\alpha_0}, \quad \text{(A12)}$$

which follows from Eq. (A9).

In practice, to obtain λ (and thus the curvature of free energy), we monitor DMFT loop convergence rate, $G(i\omega_o)^{(n+1)} - G(i\omega_o)^{(n)}$, in as many iterations as possible and then linearly fit $\ln\left(G(i\omega_o)^{(n+1)} - G(i\omega_o)^{(n)}\right)$ versus iteration index n. Here $\omega_o = \pi T$ is the lowest Matsubara frequency. For small λ, $B_{\alpha_0} \approx \lambda$. We repeat this procedure for different values of U at the same temperature T to determine $U_{WL}(T)$ in which $\lambda(U)|_T$ is minimal. It takes few iterations of the DMFT loop to enter into the linear regime given by Eq. (A12).

With IPT impurity solver, we can use data from several tens of iterations to determine the slope B_{α_0}, Fig. 8(a). The solution with CTQMC impurity solver has a statistical error and the number of iterations is limited before the difference $|G(i\omega_o)^{(n+1)} - G(i\omega_o)^{(n)}|$ becomes too small and acquires a large relative statistical error. Nevertheless, we were able to determine rather precisely the eigenvalue λ and the interaction $U^*(T)$ for which it becomes minimal, Fig. 8(b). The "instability line" corresponding to the minimum curvature of the free energy is shown in Fig. 9(a) (IPT phase diagram), and Fig. 9(b) (CTQMC phase diagram). Error bars in Fig. 9(b) are estimates of the uncertainty in the position of the instability line.

Appendix B: Boundaries of the quantum critical scaling region

In this section we explain the procedure we used to precisely determine the extent of the quantum critical region. In our previous work,[8] we defined these boundaries to enclose the region in which the mirror symmetry of the two resistivity branches is valid, but the scaling itself was found to hold in a broader region. To see at what distance from the quatum Widom line the scaling formula breaks down and the resisitivity curves do not collapse anymore, we calculate the resistivity on a dense U,T grid in a broad region around the QWL and after scaling the temperature with

$$\tilde{T} = T/T_0 = \frac{T}{c|\delta U|^{\nu z}}, \quad \text{(B1)}$$

we plot the results on Fig. 10. All the resistivity points are found to fall on two very narrow branches when $\tilde{T} \gtrsim 0.02$. Below this value of $\tilde{T}$ the resistivity points start to spread and the two branches become increasingly wider. We use this estimate to obtain the two quantum critical region boundaries (the green dashed lines on Fig. 1) given by

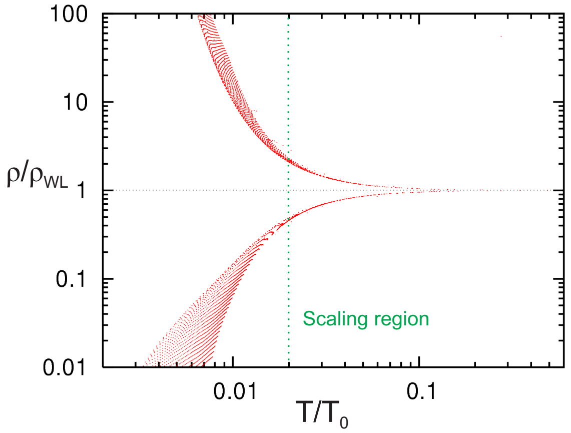

FIG. 10: Scaled resistivity in a broad region around the Quantum Widom line. The scaling formula fails below $T/T_0 \approx 0.02$.

$$|\delta U_{\text{boundary}}(T)| = \left(\frac{T}{0.02c}\right)^{\frac{1}{\nu z}} \quad \text{(B2)}$$

Appendix C: Crossover lines in the CTQMC solution

All the results presented in this paper obtained with the approximate IPT calculations are cross-checked with the numerically exact CTQMC method. The agreement between the two methods is found to be very good and all the features of the QMC results are reproduced within the IPT. Here we plot different crossover lines, Fig. 11, and use the notation from Fig. 5. The shape and direction of all these lines are found to be qualitatively the same in both approaches. The line (b) is, however, found at relatively higher temperatures in the QMC solution. Also, the light blue line (a) which corresponds to $\rho = 0.1\rho_{Mott}$ and which is roughly the Fermi liquid coherence boundary up to which the resistivity follows $\rho \propto T^2$, is at lower temperatures than in the IPT. We plot here two additional lines: (f) the quasi-particle weight at zero temperature defined by

$$Z = \left[1 - \frac{d\text{Im}\Sigma(i\omega_n)}{d\omega_n}\bigg|_{\omega_n\to 0}\right]^{-1}$$

and (g) the zero temperature magnetic susceptibility χ. Both quantities are divided by 10 to fit in the temperature range of the plot and to be more easily compared to the crossover lines. It is evident that the coherence temperature is roughly proportional to the quasi-particle weight at zero temperature, but with the prefactor 0.1, $T_{\text{FL}}(U) \sim 0.1\ Z(U)$. The quasiparticle weight Z is weakly temperature dependent for $\rho \lesssim \rho_{Mott}$.

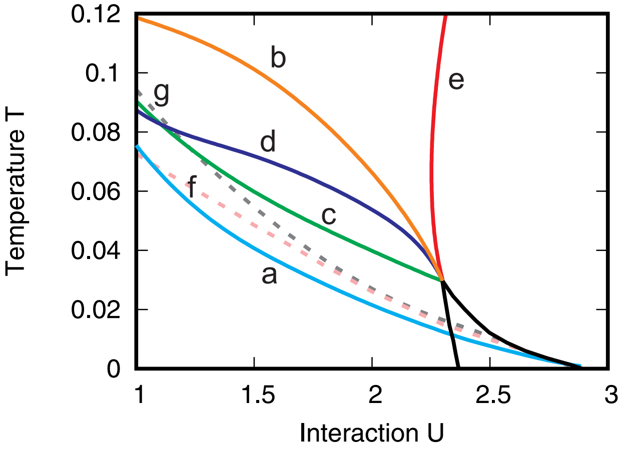

FIG. 11: Various definitions of the crossover lines. These QMC results are in good agreement with the IPT (Fig. 5).

---

[1] V. Dobrosavljević, N. Trivedi, and J. M. Valles, Jr., *Conductor-Insulator Quantum Phase Transitions* (Oxford University Press, 2012).

[2] E. Abrahams, S. V. Kravchenko, and M. P. Sarachik, Rev. Mod. Phys. **73**, 251 (2001).

[3] V. Dobrosavljević, E. Abrahams, E. Miranda, and S. Chakravarty, Phys. Rev. Lett. **79**, 455 (1997).

[4] M. M. Radonjić, D. Tanasković, V. Dobrosavljević, and K. Haule, Phys. Rev. B **81**, 075118 (2010).

[5] P. Limelette, A. Georges, D. Jérome, P. Wzietek, P. Metcalf, and J. M. Honig, Science **302**, 89 (2003).

[6] F. Kagawa, K. Miyagawa, and K. Kanoda, Nature **436**, 534 (2005).

[7] D. Tanasković, K. Haule, G. Kotliar, and V. Dobrosavljević, Phys. Rev. B **84**, 115105 (2011).

[8] H. Terletska, J. Vučičević, D. Tanasković, and V. Dobrosavljević, Phys. Rev. Lett. **107**, 026401 (2011).

[9] G. G. Simeoni, T. Bryk, F. A. Gorelli, M. Krisch, G. Ruocco, M. Santoro, and T. Scopigno, Nature Physics **6**, 503 (2010).

[10] A. Georges, Annalen der Physik **523**, 672 (2011).

[11] A. Georges, G. Kotliar, W. Krauth, and M. J. Rozenberg, Rev. Mod. Phys. **68**, 13 (1996).

[12] P. Werner, A. Comanac, L. de Medici, M. Troyer, and A. J. Millis, Phys. Rev. Lett. **97**, 076405 (2006).

[13] K. Haule, Phys. Rev. B **75**, 155113 (2007).

[14] N. E. Hussey, K. Takenaka, and H. Takagi, Philos. Mag. **84**, 2847 (2004).

[15] X. Deng, J. Mravlje, R. Žitko, M. Ferrero, G. Kotliar, and A. Georges, ArXiv: 1210.1769 (2012).

[16] T. Pruschke, D. Cox, and M. Jarrell, Phys. Rev. B **47**, 3553 (1993).

[17] M. J. Rozenberg, G. Kotliar, H. Kajueter, G. A. Thomas, D. H. Rapkine, J. M. Honig, and P. Metcalf, Phys. Rev. Lett. **75**, 105 (1995).

[18] G. Kotliar, E. Lange, and M. J. Rozenberg, Phys. Rev. Lett. **48**, 5180 (2000).

[19] J. H. Mooij, Physica Status Solidi (a) **17**, 521 (1973).

[20] G. Moeller, V. Dobrosavljević, and A. E. Ruckenstein, Phys. Rev. B **59**, 6846 (1999).

[21] M. J. Case and V. Dobrosavljević, Phys. Rev. Lett. **99**, 147204 (2007).

[22] P. Sémon and A.-M.S. Tremblay, Phys. Rev. B **85**, 201101(R) (2012).

[23] S. Sachdev, *Quantum Phase Transitions* (Cambridge University Press, Cambridge, 1999).

[24] B. J. Powell and R. H. McKenzie, J. Phys.: Condens. Matter **18** (2006).

[25] G. Sordi, P. Sémon, and A.-M.S. Tremblay, Scientific Reports **2**, 547 (2012).

[26] H. Park, K. Haule, and G. Kotliar, Phys. Rev. Lett. **101**, 186403 (2008).

[27] G. Sordi, A. Amaricci, and M. J. Rozenberg, Phys. Rev. B **80**, 035129 (2009).